(2)

MEMORANDUM REPORT BRL-MR-3885

BRL

ENERGY-EFFICIENT PENETRATION OF TARGETS

KONRAD FRANK
JOHN A. ZOOK

FEBRUARY 1991

U.S. ARMY LABORATORY COMMAND

BALLISTIC RESEARCH LABORATORY
ABERDEEN PROVING GROUND, MARYLAND

NOTICES

Destroy this report when it is no longer needed. DO NOT return it to the originator.

Additional copies of this report may be obtained from the National Technical Information Service, U.S. Department of Commerce, 5285 Port Royal Road, Springfield, VA 22161.

The findings of this report are not to be construed as an official Department of the Army position, unless so designated by other authorized documents.

The use of trade names or manufacturers' names in this report does not constitute indorsement of any commercial product.

REPORT DOCUMENT PAGE

Form Approved
OMB No. 0704-0188

1. AGENCY USE ONLY *(Leave blank)*	2. REPORT DATE	3. REPORT TYPE AND DATES COVERED
	February 1991	Final Oct 85 - Sep 89

4. TITLE AND SUBTITLE
Energy-Efficient Penetration of Targets

5. FUNDING NUMBERS
1L162618AH80

6. AUTHOR(S)
Konrad Frank
John A. Zook

7. PERFORMING ORGANIZATION NAME(S) AND ADDRESS(ES)

8. PERFORMING ORGANIZATION REPORT NUMBER

9. SPONSORING/MONITORING AGENCY NAMES(S) AND ADDRESS(ES)
Director
U.S. Army Ballistic Research Laboratory
ATTN: SLCBR-DD-T
Aberdeen Proving Ground, MD 21005-5066

10.SPONSORING/MONITORING AGENCY REPORT NUMBER
BRL-MR-3885

11. SUPPLEMENTARY NOTES

12a. DISTRIBUTION/AVAILABILITY STATEMENT
Approved for public release; distribution is unlimited.

12b. DISTRIBUTION CODE

13. ABSTRACT ***(Maximum 200 words)***

In general, the performance of a kinetic energy (KE) penetrator against most targets increases with velocity regardless of the particular penetrator-target interaction mode. It is possible to show that there exists an optimum velocity which maximizes the performance of an impacting penetrator for a given expenditure of energy. Simple graphical methods are described that determine the optimum velocity from general performance-velocity plots. These graphical methods may also be applied to experimental data alone. In addition, simple analytic models which describe the velocity dependent penetration/perforation performance of KE penetrators are examined and extended. These models may be used to assess explicitly the influence of parameters such as target strength and density, and penetrator mass, strength and density. For some models in this analysis, the explicit relations between the optimum striking velocity for a specified KE value and the penetrator-target parameters are described.

14. SUBJECT TERMS
kinetic energy, armor, penetration projectiles, high velocity, hypervelocity impact, optimum velocity

15. NUMBER OF PAGES
40

16. PRICE CODE

17. SECURITY CLASSIFICATION OF REPORT	18. SECURITY CLASSIFICATION OF THIS PAGE	19. SECURITY CLASSIFICATION OF ABSTRACT	20. LIMITATION OF ABSTRACT
UNCLASSIFIED	UNCLASSIFIED	UNCLASSIFIED	UL

NSN 7540-01-280-5500
Standard Form 298 (Rev. 2-89)
Prescribed by ANSI Std. 239-18 298-102

THIS PAGE INTENTIONALLY BLANK

TABLE OF CONTENTS

THIS PAGE INTENTIONALLY BLANK

LIST OF FIGURES

THIS PAGE INTENTIONALLY BLANK

I. INTRODUCTION

When a kinetic energy (KE) projectile is shot against a homogeneous barrier (target), its performance is, in general, a function that increases monotonically with impact velocity. The performance may be taken as penetration depth, a limit thickness just perforated with negligible residual mass/velocity (energy) behind the barrier, or some other appropriate measure of effectiveness. Nearly all physical penetrator-target interactions admit a performance description in terms of a relation like:

$$P = L \cdot S(V, \rho_t, \rho_p, H, Y, f, \ldots) , \qquad (1)$$

where P is the performance, L is a characteristic dimension of the penetrator, and S is a characteristic function that depends on velocity V, the density of the target material ρ_t, and of the penetrator ρ_p, the dynamic strength of the target material H, and of the penetrator Y, the fineness ratio f (the length to diameter ratio L/D) and possibly other characteristics describing the interaction. But, S is not explicitly dependent on the length or on the diameter of the penetrator.

The function S increases with velocity, generally in a monotonic fashion, except in cases where the character of the penetrator-target interaction changes in some velocity regime. For example, at some velocity, the penetrator may change its form rather suddenly, say by breaking up, and the S function may dip in this case and then continue again to increase. The formalism introduced by Equation 1 implies geometric scaling to be applicable. Inter alia, this means that the same performance, P, can be achieved either with a larger penetrator at a lower velocity (smaller S function value), or a smaller penetrator at a higher velocity (larger S function value). By applying additional constraints, like keeping the impact energy constant, it is possible to show that for most S functions, there exists an optimum velocity where the performance of the penetrator, subject to that constraint, is maximized.

This methodology was discovered at the BRL circa 1976 and has been used effectively in many studies. It has been presented in "closed" meetings, reported briefly on some of its main features (Wright, 1983[1]) and its main conclusions have been used in commenting on the significance of some recent hypervelocity results (Silsby, 1984[2]). It was presented at The 1986 Hypervelocity Impact Symposium held in San Antonio, TX. The proceedings of this symposium have been published in the International Journal of Impact Engineering[3]. This report is an expanded version of the paper presented at the 1986 symposium.

II. KE PROJECTILE PERFORMANCE SUBJECT TO CONSTRAINTS

One constraint of interest is that of constant penetrator energy. With some launcher systems, like electromagnetic guns (EMG), it is possible, in principle, to launch projectiles over a very wide range of mass and velocity holding the kinetic energy constant, without a significant impact on the system size and cost. The kinetic energy of a projectile is simply:

$$E = \frac{1}{2}\frac{\pi D^2}{4} L \rho_p V^2 = f\frac{D^3 V^2}{8/(\pi \rho_p)} = f\frac{D^3 V^2}{K^3} \quad . \tag{2}$$

for a cylindrical projectile of diameter D, length L and material density ρ_p moving with the velocity V. From Equation 2, we may calculate the diameter of a constant energy projectile as:

$$D = K\frac{E^{1/3}}{f^{1/3} V^{2/3}} \quad . \tag{3}$$

With L = f D and Equation 1, we obtain:

$$P = K\frac{f^{2/3} E^{1/3}}{V^{2/3}}\, S(V, \ldots) \quad . \tag{4}$$

The extrema of Equation 4 are found by solving $\partial P/\partial V = P' = 0$. The equation for the extrema of P, subject to the constraint E = constant and f = constant is:

$$V\frac{\partial S}{\partial V} = VS' = \frac{2}{3} S \quad for\ V = V_{opt} \quad . \tag{5}$$

The solution of Equation 5 yields the velocity (or velocities) where P' = 0, and therefore, P assumes an extremum. For the kind of S functions described earlier, this extremum is a maximum of P subject to the constraints noted above.

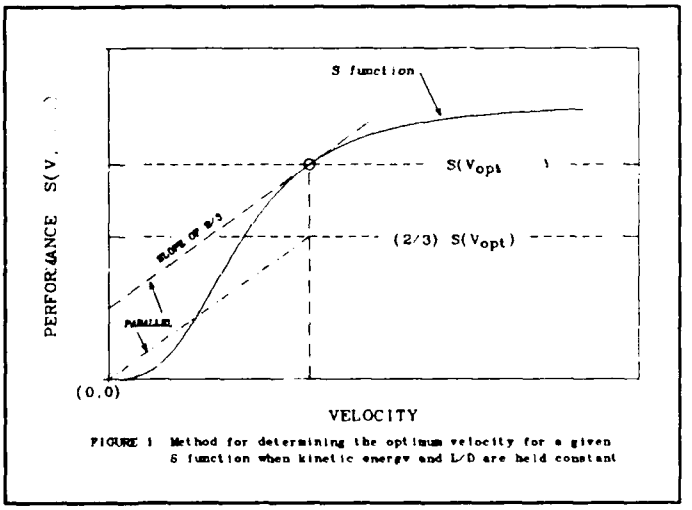

FIGURE 1 Method for determining the optimum velocity for a given S function when kinetic energy and L/D are held constant

The form of Equation 5 suggests a simple graphical means to find the optimum when the S function is not given as an explicit analytic function of V, but exists only as a graph of experimental data. A line drawn from the origin (0,0) to the 2/3 value of $S(V_{opt})$ is parallel to the tangent of the S-V curve at V_{opt}, as illustrated in **Figure 1.**

The application of this graphical technique to real experimental data obtained in the velocity range between 1.2 km/s and 4.6 km/s illustrates the procedure in more detail. The data of Silsby (1984[2]) are summarized in Table 1. The S function values in the table are calculated based on solving Equation 4 (or Equation 1) explicitly for the S function. **Figure 2** shows a plot of these data with a curve manually fitted through the points. Applying the above technique to these data, as shown in the figure, we find with only a few trials an optimum velocity of about 2.2 km/s. This corresponds to the optimum performance if the kinetic energy and the L/D are held constant. Note that $S(V_{opt}, ...)$ is only about 1.35, or about 85% of the S value at 4.5 km/s.

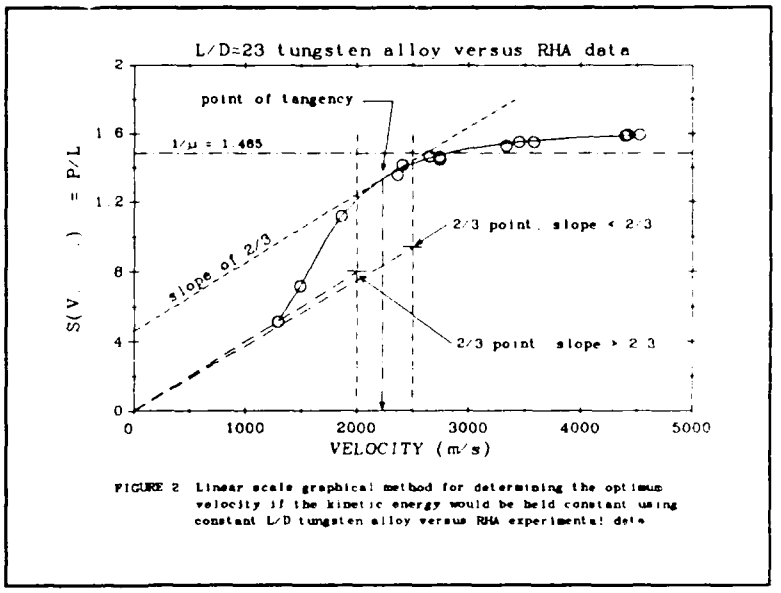

FIGURE 2 Linear scale graphical method for determining the optimum velocity if the kinetic energy would be held constant using constant L/D tungsten alloy versus RHA experimental data.

TABLE 1. Tungsten Alloy Rods (L/D = 23, ρ=17.3 g/cc) Versus RHA
(8th International Symposium on Ballistics - G. Silsby)

Mass (g)	Length (mm)	Diameter (mm)	Velocity (m/s)	Depth (mm)	S(V, ...) (P/L)
100.01	155.78	6.87	1291	80.0	0.5135
98.58	155.83	6.82	1494	112.0	0.7187
98.63	155.83	6.83	1865	174.5	1.1198
46.20	121.79	5.28	2365	165.2	1.3564
47.28	121.79	5.35	2409	172.3	1.4147
96.96	155.83	6.76	2653	228.5	1.4663
95.16	155.83	6.70	2742	228.0	1.4631
43.86	121.79	5.15	2746	176.3	1.4476
97.82	155.83	6.80	3335	237.9	1.5267
96.73	155.83	6.70	3449	241.5	1.5498
46.02	121.79	5.27	3580	188.6	1.5486
94.84	155.75	6.69	4398	246.9	1.5852
99.54	155.83	6.86	4415	248.1	1.5921
45.41	121.69	5.24	4525	193.7	1.5918

Another set of constraints that is useful minimizes the energy required to achieve equal performance. By taking P constant and f constant and proceeding in the same manner as before, we again obtain Equation 5. The optimum velocity (representing the minimum energy to achieve the same performance P) is found by solving Equation 5 as before.

The next case of interest is that of a projectile with the diameter and kinetic energy held constant. For simplicity, we will consider here only the special case where S is not dependent on f. Calculating f from the projectile energy:

$$f = \frac{K^3 E}{D^3 V^2} \quad , \tag{6}$$

and using:

$$P = f\, D\, S(V, \ldots) = \frac{K^3 E\, D^{-2}}{V^2} S(V, \ldots) \tag{7}$$

and setting $\partial P/\partial V = P' = 0$, we obtain the extrema condition to be:

$$V\, S' = 2\, S \quad \text{for} \quad V = V_{opt} \quad . \tag{8}$$

A graphical solution analogous to that outlined for Equation 5 can be developed (as illustrated in **Figure 3**) but not all S curves yield a solution. A unique solution requires an S-V curve with a relatively steep slope.

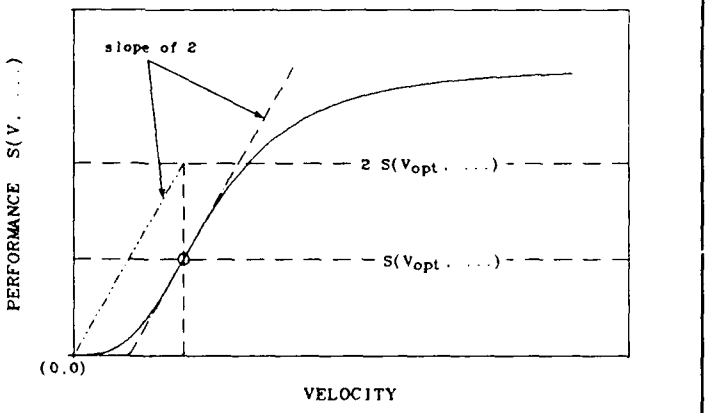

FIGURE 3 Method for determining the optimum velocity for a given S function when kinetic energy and diameter are held constant.

An even simpler geometric construction is possible if the data are plotted using logarithmic scales, i.e, $\ell n(P)$ vs. $\ell n(V)$. Since the log transformation is monotonic, the extrema of P vs. V occur at the same values as those of $\ell n(P)$ vs. $\ell n(V)$. Following the same procedures as used above, we find that maximum performance at constant energy and constant L/D occurs when the $\partial(\ln P)/\partial(\ln V) = 2/3$ and the maximum for constant energy and constant diameter occurs when $\partial(\ell n P)/\partial(\ell n V) = 2$. In all cases, the underlying assumption is that geometric scaling applies.

An example of the graphical method of finding maximum performance for constant energy and constant L/D using logarithmic scales is shown in **Figure 4**. The data are the same as that of Figure 2 and the curve is manually fitted through the points. A reference line which has a slope of 2/3 is shown and a line parallel to it but tangent to the data curve yields the point of maximum performance if the kinetic energy had been held constant. Again, the velocity corresponding to this point is about 2.2 km/s.

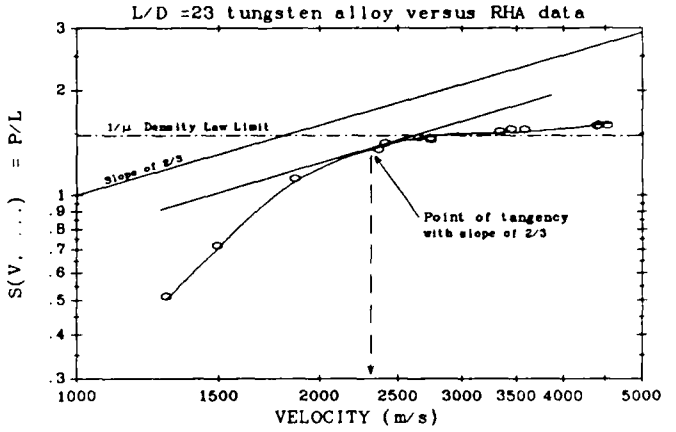

FIGURE 4 Logarithmic scale graphical method for determining the optimum velocity if the kinetic energy would be held constant using constant L/D tungsten alloy versus RHA experimental data

The methodology outlined above is most general in nature. The S curves may be analytic forms, may be given in graphical form based on experimental data or may be generated by numerical methods.

III. PENETRATION OF HOMOGENEOUS TARGETS

Next, we shall provide some examples using explicit analytic formulations that are suitable throughout most of the hyper-velocity regime. For simplicity, we will restrict the discussion to the most simple case - penetration of homogeneous targets. First, we deal with the short penetrator of constant mass. Vitman and Zlatin (1962)[4] and Belyakov, Vitman and Zlatin (1962[5], 1963[6]) have shown that the resistance to penetration is given by:

$$H + k_0 \rho_t V^2 , \qquad (9)$$

where H is a dynamic material property which is only weakly dependent on velocity They showed that the resulting simple relation:

$$P = L \frac{1}{2k_0} \frac{\rho_p}{\rho_t} \ln\left(1 + 2k_0 Z_0^2\right) \quad \text{where } Z_0^2 = \frac{\rho_t V_0^2}{2H} \qquad (10)$$

and V_0 is the striking velocity, describes the penetration behavior of different penetrator and target materials rather well to very high velocities. In the following, we take $2k_0 = 1$ and add to Equation 9 a term that accounts for the effect of the target material moving in front of the penetrator in a non-steady

flow (Goodier, 1964[7]; Hanagud and Ross, 1971[8]; Byrnside, Torvik and Swift, 1972[9]; Johnson, 1972[10]; Tate, 1979[11]). In passing, we note that the target resistance term is directly related to the work required to make a unit volume cavity in the target (Johnson, 1972[10]; Hill, 1980[12]; Hopkins, 1960[13]). For plastically deforming materials, a good estimate for it can be obtained from bi-linear approximations to quasi-static stress-strain data (Hill, 1980[12]; Hopkins, 1960[13]).

The resulting relation for a non-deforming constant mass penetrator is given by (Goodier, 1964[7]):

$$\frac{P(Z_0, Z)}{L} = \frac{\rho_p}{\rho_t}\left(1+\frac{\rho_t D}{3\rho_p L}\right) \ln\left(\frac{1+Z_0^2}{1+Z^2}\right) \qquad (11)$$

where the quantity $\rho_t D/(3\rho_p L)$ accounts for the additional accelerated target mass in front of the penetrator (the factor 1/3 implies a hemispherical cap of affected target material in front of the penetrator). Note that $Z^2 = \rho_t V^2/(2H)$. (See Appendix A for derivation of Equation 11.)

Setting $S(Z_0,Z)$ equal to the right side of Equation 11 (see Equation 1), setting $Z = 0$, taking the derivative of $S(Z_0,0)$ with respect to Z_0 and making appropriate substitutions into Equation 5 (replacing V by Z since Z is directly proportional to V), the optimum Z_0 at constant kinetic energy is found by solving

$$\left(1+Z_0^2\right) \ln\left(1+Z_0^2\right) - 3Z_0^2 = 0 \qquad (12)$$

which has the approximate solution of $Z_0 = 3.975$.

For a target material of armor steel, the value of $2H/\rho_t$ is about $(1000\ m/s)^2$, so that optimum penetration performance occurs at an impact velocity near 4000 m/s. The curve in the vicinity of the optimum velocity is nearly flat. Therefore, near optimum penetration for constant impact energy can be achieved over a wide range of velocities. This is illustrated in **Figure 5** for a one megajoule L/D=2 iron penetrator impacting armor steel.

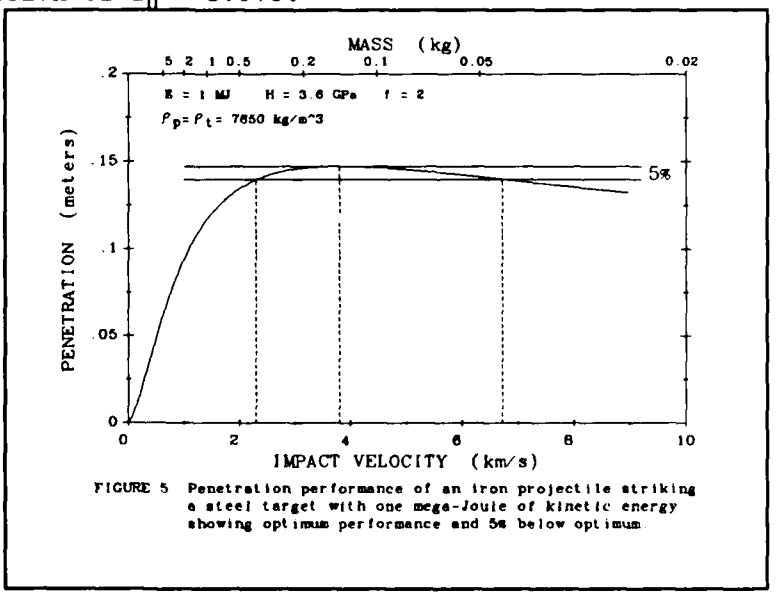

FIGURE 5 Penetration performance of an iron projectile striking a steel target with one mega-Joule of kinetic energy showing optimum performance and 5% below optimum

Of much greater interest in practice, are deforming or eroding penetrators. There have been many papers published on this subject beginning with the classical works of Alekseevskii and Tate in the 1960's (Alekseevskii, 1966[14]; Tate, 1967[15],1969[16]) with more refinements which remove some of the earlier limitations being added even today (Tate, 1986[17]). In the following, we shall present formulations (using a consistent notation) which we have found useful.

Following the basic ideas of Christman and Gehring (1966[18]), the penetration of a long deforming/eroding rod penetrator may be separated according to the important identifiable phases or stages of the penetration process. For example,

$$\underset{\text{stage 1}}{} \qquad \underset{\text{stage 2}}{} \qquad \underset{\text{stage 3}}{}$$

$$P(Z_0, Z) = m_1 D\, S_{D1}(Z_0, Z_1) + (L - m_2 D)\, S_1(Z_1, Z_2) + m_3 D\, S_{D2}(Z_2, Z) \tag{13}$$

where $Z_0 > Z_1 > Z_2 > Z \geq 0$. The first term describes the transient where m_1 diameters of the rod are "used" up. The second term is the quasi-steady state phase which erodes the length $L - m_2 D$ of the rod. The final stage is the penetration by a $m_3 D$ constant mass penetrator. It is not obvious that the equation described above can always be constructed in a consistent manner. However, we have found that the following simpler form gives satisfactory results:

$$P(Z_0, Z) = (L - mD)\, S_i(Z_0, Z) + mD\, S_D(Z_0, Z) \ . \tag{14}$$

This may be considered an approximation, in the spirit of Christman and Gehring, which holds over the whole velocity range, including low velocities where their original formulation fails. The diameter function S_D, is based on Equation 11:

$$S_D(Z_0, Z) = \left(\frac{\rho_p}{\rho_t} + \frac{1}{3m} \right) \ln\left(\frac{1 + Z_0^2}{1 + Z^2} \right) \ . \tag{15}$$

Here, m is considered an adjustable parameter with typical values between 0.5 and 2. In this formulation, S_D attempts to describe both stage 1 and stage 3 of the penetration process. When used by itself (non-eroding long rod penetrator), m is set equal to L/D. For the S function denoted as $S_i(Z_0, Z)$, we will present several functions appropriate to special cases of interest. (More details concerning these S functions are in Appendix B.)

The first function, S_1, is that for a penetrator with no strength ($Y \to 0$, using the Tate/Alekseevskii notation) representing, for example, a non-stretching jet (Rostoker, 1953[19]). Since such a penetrator does not slow down during penetration, S is a function of Z_0 only, and the process terminates when the length L - m D is used up.

$$S_1(Z_0) = \frac{Z_0\sqrt{Z_0^2+1-\mu^2} - \mu}{\mu\left(1+Z_0^2\right)} \quad for\ Z_c < Z_0 \leq \infty \tag{16}$$

and $S_1(Z_0)=0$ for $0<Z_0<Z_c=\mu$, where $\mu^2 = \rho_t/\rho_p$ (Tate/Alekseevskii notation) and Z_c is the normalized cut-off velocity below which no penetration occurs. See Appendix B for some background on the derivation.

The second S function for the length term is Tate's special case for Y = H, applicable to the entire velocity range from 0 to infinity. (See Appendix B for some background on the derivation.)

$$S_2(Z_0, Z) = \frac{1}{\mu}\left(1 - e^{\left(\frac{Z^2-Z_0^2}{\mu(1+\mu)}\right)}\right) . \tag{17}$$

If we subject $S_2(Z_0,0)$ to the optimization procedure for constant energy and L/D , i.e., solve Equation 5, we obtain the transcendental equation:

$$\ell n(1+3y) - y = 0 , \tag{18}$$

where $y = \frac{Z_{opt}^2}{\mu(1+\mu)}$ which has the solution y = 1.9038. With μ < 1 (high density penetrator impacting lower density targets), the optimum velocity $V_{opt} = Z_{opt}\sqrt{\frac{2H}{\rho_t}}$ can be considerably lower than that for the case of the constant mass penetrator discussed earlier.

Tate also gave a solution for Y equal to fractional values of H, but only for the restricted case of μ=1 (target and penetrator densities equal). Using an approximate solution of the Tate/Alekseevskii "Bernoulli equation", but with a better approximation than that of Alekseevskii's, that preserves the cut-off velocity, we developed a closed form solution for the case Y = H/(2+μ), which is:

$$S_3(Z_0, 0) = \frac{1}{\mu}\left(1 - \frac{1+\mu}{a_0} + \frac{e^{(\mu-a_0)}}{a_0}\right) \tag{19}$$

for $a_c<a_0\leq \infty$ and $S_3(Z_0,0)=0$ for $0<a_0\leq a_c$ where $a_0 = Z^2\left(\frac{2+\mu}{\mu(1+\mu)}\right)$ and $a_c = \mu$. See Appendix B for the derivation.

More functions of this kind can be given, but only for Y values that are smaller than that for S_3. Since the S_1 and S_3 curves are not greatly separated, these new functions are not of great practical value. What is needed, however, is a family of functions that fill the large gap between S_2 and S_0. Functions of this kind can be generated by using what must be considered a radical, if not

bizarre, approximation to the variable mass penetrator problem.

In experiments with high density long rod penetrators against finite thickness plates, it is noted that the length of rod lost and eroded is proportional to the target thickness perforated. If systematic variations with velocity are ignored, we can start with:

$$L_x = L_m - rx = L_0 - mD - rx \tag{20}$$

where L_x is the instantaneous rod length, L_0 is the initial length, D is penetrator diameter, x is the penetration depth and m and r are dimensionless constants. Differentiating Equation 20 and noting that dL/dt = -(v-u) where (using Tate's notation) v is the instantaneous velocity of the rear of the penetrator and u = dx/dt is the penetrator-target interface velocity, we find that r = (v-u)/u. (This will be referred to as the constant v/u approximation.)

Next, the kinematics of the eroding rod are approximated by using Tate's "Bernoulli equation" and noting that $Y = -\rho_p L\, dv/dt$ (see Appendix B):

$$-\rho_p L\frac{dv}{dt}+\frac{1}{2}\rho_p(v-u)^2 = H+\frac{1}{2}\rho_t u^2 \ . \tag{21}$$

This is now interpreted as an equation of motion and, as with the S_D function, supplemented on the right-hand side with the added target mass term:

$$-\rho_p L\frac{dv}{dt}+\frac{1}{2}\rho_p(v-u)^2 = H+\frac{1}{2}\rho_t u^2+\frac{1}{3}D\rho_t\frac{du}{dt} \ . \tag{22}$$

With the earlier constant v/u approximation, we have v = u(1+r), $(v-u)^2 = (ru)^2$ and $\frac{du}{dt} = \frac{dv/dt}{1+r}$. Therefore, Equation 22 can be integrated after dividing through by ρ_p and substituting for L (using Equation 20), $(v-u)^2$ and du/dt and then separating variables. By defining:

$$c^2 = \frac{\mu^2-r^2}{\mu^2(1+r^2)} \quad ; \ 0<c^2<1 \ , \tag{23}$$

$$b = \frac{r(1+r)}{\mu^2-r^2} \ >0 \ , \tag{24}$$

$$e = \frac{\rho_t D}{3\rho_p L_m} = \frac{\rho_t D}{3\rho_p(L_0-mD)} = \frac{\mu^2}{3(f-m)} \tag{25}$$

and $d = \frac{e}{1+r}$, the result is: (26)

$$S_4(Z_0, Z) = \frac{1+d}{r}\left(1-\left(\frac{1+c^2Z^2}{1+c^2Z_0^2}\right)^b\right) . \qquad (27)$$

The primary parameter is r which is the proportionality factor between rod mass loss and penetration. It can be shown that as $r \rightarrow \mu$, $S_4 \rightarrow S_2$. Also, as $r \rightarrow 0$, the differential equation (Equation 22) approaches that for S_D. Therefore, the range $0< r <\mu$ generates curves between S_D and S_2. The physical relevance of Equation 27 can not be assessed at this time, so it should not be taken too seriously. The constant v/u approximation which is the basis for deriving S_4 is certainly open to severe criticisms. Nevertheless, the collection of S functions given above, together with Equation 14, allows for some interesting parametric studies.

The character of these functions is shown in **Figure 6**. The functions S_1, S_2, S_3 and S_4 (with $r\approx\mu$) tend to the high velocity limit of $1/\mu$ while S_4 with $r\approx 0$ approaches the S_D function. The S_D function tends toward infinity in a logarithmic fashion. See Appendix C for some additional examples of parametric variation.

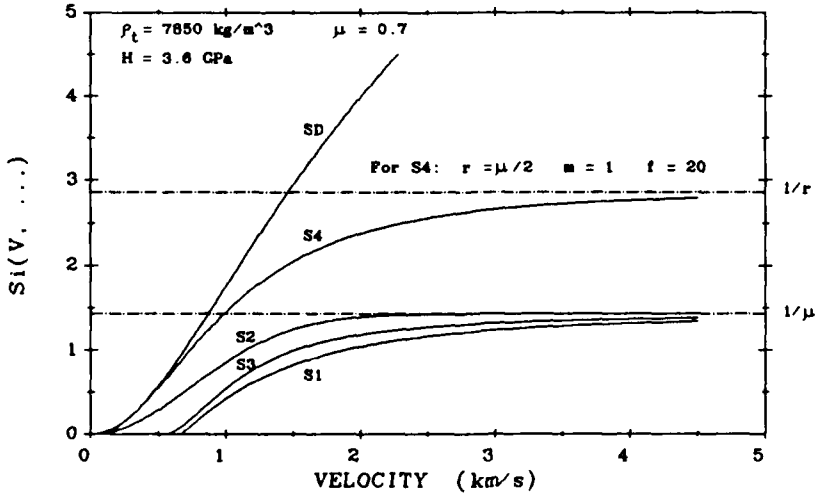

FIGURE 6 Characteristic S functions related to penetrator length (S1 - S4) and related to penetrator diameter (SD).

IV. APPLICATIONS

An example of the application of these analytical forms is shown in **Figure 7**. This is a plot of the final penetration P (Equation 14 with S_i being replaced by S_1 through S_4 for each curve respectively) as a function of the impact velocity for the case where E=1 MJ, f=20, μ=0.7, r=μ/2, m=1 and ρ_t = 7850 kg/m^3 (armor steel). The performance (note that the ordinate is P and not P/L) maxima (the peak of each curve) occur at P = 0.30, 0.41, 0.34, and 0.64 meters with the optimum velocities of 2.0, 1.5, 1.72 and 1.52 km/s for the functions S_1, S_2, S_3 and S_4 respectively. The non-dimensional Z values are 2.09, 1.57, 1.79 and 1.59 respectively. The penetration at the optimum velocity increases with penetrator strength Y since the functions $S_1<S_3<S_2<S_4$ are associated with the penetrator strengths $0 = Y_1<Y_3<Y_2<Y_4$, and the corresponding cut-off velocities decrease. If the dynamic strength of the target material, H, is increased, the performance maxima (indicated in Figure 7 by a tic mark at the peak of each curve) decrease in value and shift to higher velocities.

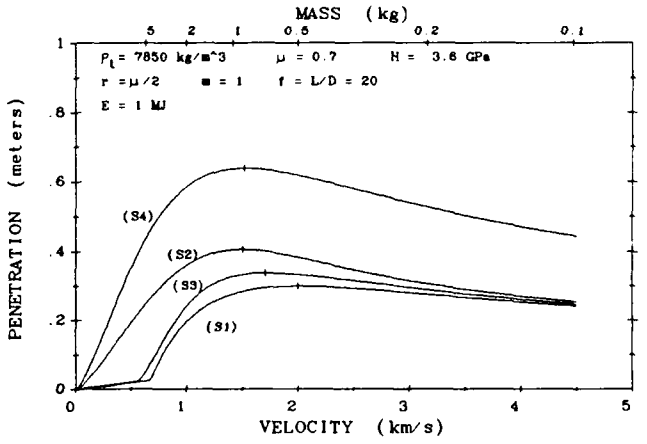

FIGURE 7 Two phase penetration performance (f - m) $S_i(Z_0,0)$ + mD $S_D(Z_0,0)$. The mark at the peak of each curve shows the velocity for optimum penetration.

The curves in Figure 7 are plots of Equation 14 with E = 1 MJ. If the ordinate of the graph is re-scaled and labeled as $P/(E^{1/3})$ in units of $m/(MJ)^{1/3}$, Figure 7 may be used for other constant energy levels as well. For example, with E = 8 MJ or 27 MJ, the P-values of Figure 7 would be 2 times or 3 times higher respectively.

The experimental data from Table 1 (Section II) is for a tungsten alloy (WA) penetrator fired against RHA. The dynamic strength for WA is between 1 and 2 GPa and the density is 17300 kg/m^3. The dynamic strength of RHA is between 4 and 6 GPa and its density is 7850 kg/m^3. For these densities, $\mu = \sqrt{\rho_t/\rho_p} = \sqrt{0.4537} = 0.6736$. The criterion for developing the S_3 function is that Y = H/(2 + μ). Substituting the values of 4 and 6 GPa for H and the value for μ yields Y = 1.5 and 2.2 GPa respectively. Applying Equation 14 with S_3 for S_i, taking m = 1, k_o = 1, $k_t = k_p$,

(see Appendix B) and f=23, the curves of **Figure 8** are produced (taking H = 4, 6 or 8 GPa). The data points are those from Table 1. Above 1800 m/s, the data lie between the curves for H = 4 and H = 6 GPa. The two points below 1800 m/s lie between the H = 6 and H = 8 GPa curves. These two shots were fired at the BRL while the rest were fired at the hypervelocity range facility at Tullahoma, TN. Whether the inconsistency is due to experimental differences or that the criterion for the S_3 function is not applicable is not known at this time. It seems certain that a value of 8 GPa for the dynamic strength of RHA is much too high.

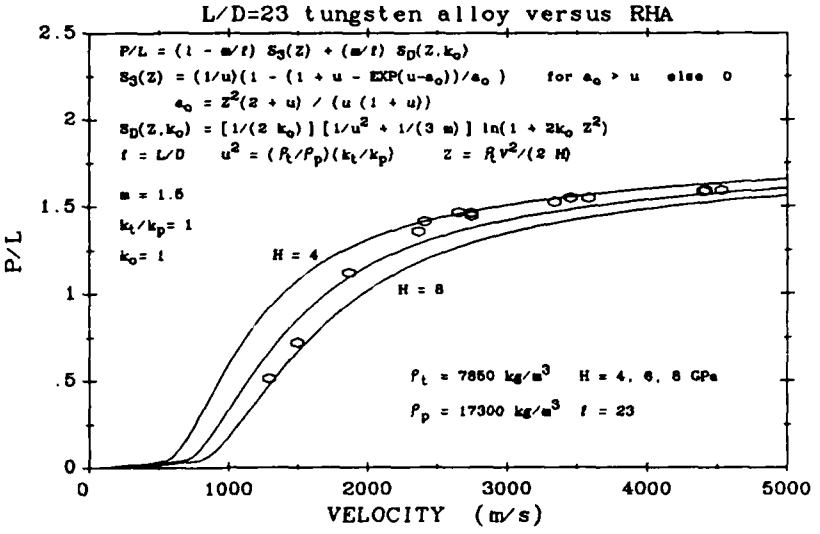

FIGURE 8 Bracketing the data of Table 1 using the two phase penetration performance of $S_D(Z_0,0)$ and $S_3(Z_0,0)$ with H = 4, 6 and 8 GPa.

There are other ways of getting a curve to fit the data. For example, shifting the S_3 function to the right by 390 m/s, taking m = 1.404, and H = 4 GPa results in the curve of **Figure 9**. It is not clear that shifting the S_3 function is justified. What is needed is a set of data for one or more penetrators for striking velocities from about 200 m/s out to 4500 m/s at intervals less than 500 m/s

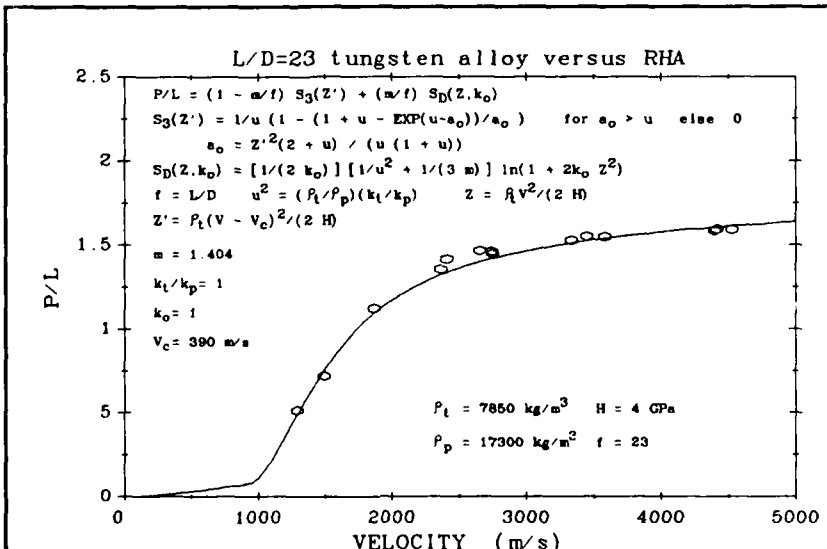

FIGURE 9 Fitting the data of Table 1 using the two phase penetration performance of $S_D(Z_0,0)$ and a shifted $S_3(Z_0,0)$ with H = 4 GPa.

where both Y and H are known to a good degree of certainty.

In applying these equations to a particular situation, one should keep in mind that increasing the value of H will shift the curve to the right. Increasing the value of ρ_t shifts the curve down. Increasing the value of Y will shift the curve to the left. Increasing ρ_p shifts the curve up. In addition, one should be cognizant of the following which are based on experimental experience with metal impacting metal interactions.

(1) If $Y \leq H$ the penetrator will erode during penetration and for $V_0 \leq V_c = \sqrt{\frac{H-Y}{k_p \rho_p}}$ (see Appendix B, equation B-6) the depth of penetration is only a few milli-meters.

(2) If $Y > H$, the penetrator remains rigid - doesn't deform unless $V > \sqrt{\frac{Y-H}{k_t \rho_t}}$ where V is the instantaneous velocity.

(3) For a given set of conditions which include normal impact, a penetrator will defeat a finite thickness target with a substantial residual velocity when the target thickness equals the depth of penetration into the semi-infinte target.

V. CONCLUDING REMARKS

These examples illustrate some of the capabilities of the methodology presented in this paper. Another obvious application is the first order analysis of multiple penetrators, that is, the performance of one long penetrator may be compared to N shorter penetrators of equal material length and mass (segmented penetrators). This last case can not consider the effects of separation between penetrator segments, nor can it account for penetrator mass remaining in the crater from previous impacts in a successive series of impacts. Never-the-less, it provides for the initial assessment of the efficacy of segmented penetrators, especially in the higher velocity regime.

Finally, we will attempt to answer one obvious question. In this day and age of "super computers" and refined computational techniques, why bother with

approximate closed form analytic expressions? In the exploratory stages of research and development, there are many occasions where a large number of parametric investigations need to be made. The requirement is not necessarily the non-plus-ultra in accuracy, but a consistent set of equations that reflects the major trends reasonably well and does not misrepresent the important physical interdependencies. For this kind of use, the formulations presented in this paper prove to be superior. At their best, they provide reasonable first estimates requiring a minimal amount of material parameters and of computational resources. At their worst, one can delegate them into the realm of semi-empirical fitting formulas, but with parameters that have some direct physical relation to the penetrator-target interaction process.

REFERENCES

1. T. Wright, "A Survey of Penetration Mechanics for Long Rods", J. Chandra and J.E. Flaherty (Editors), Proceedings of the Army Research Office Workshop on Computational Aspects of Penetration Mechanics, Ballistic Research Laboratory, Aberdeen Proving Ground, MD, 27-29 April 1982, C. A. Brebbia and S. A. Orzag (Editors), Lecture Notes in Engineering, Vol. 3, Springer-Verlag, 1983.

2. Silsby, G. F., "Penetration of Semi-Infinite Steel Targets by Tungsten Long Rods at 1.3 to 4.5 km/s", Proceedings of the Eighth International Symposium on Ballistics, Orlando FL, 1984.

3. Konrad Frank and John Zook, "Energy-Efficient Penetration and Perforation of Targets in the Hypervelocity Regime", Proceedings of The 1986 Hypervelocity Impact Symposium, International Journal of Impact Engineering, Vol. 5, 1987, pp 277-284.

4. Vitman, F. F. and Zlatin, N.A., "Collision of Deformable Bodies and its Modelling: I. Status and Theory of the Problem", Zhurnal Tekhnicheskoi Fiziki, Vol. 33, No. 8, 1962, pp 982-989.

5. Belyakov,L. V., Vitman, F.F. and Zlatin, N.A., "Collision of Deformable Bodies and its Modelling: II. The Modelling of the Impact of a Sphere and a Half-Space", Zhurnal Tekhnicheskoi Fiziki, Vol. 33, No. 8, 1962, pp 990-995.

6. Belyakov,L. V., Vitman, F.F. and Zlatin, N.A., "Collision of Deformable Bodies and its Simulation : III. Similitude of the Instantaneous Parameter Values for the Original and Modelling Processes", Zhurnal Tekhnicheskoi Fiziki, Vol. 34, No. 3, 1963, pp 519-522.

7. Goodier, J. N., "On the Mechanics of Indentation and Cratering in Solid Targets of Strain-Hardening Metal by Impact of Hard and Soft Spheres", Proceedings of the Seventh HyperVelocity Impact Symposium, Volume III - Theory, Orlando FL , 1964.

8. Hanagud, S. and Ross, B., "Large Deformation, Deep Penetration Theory for a Compressible Strain-Hardening Target Material", AIAA Journal, Vol. 9, No. 5, 1971, pp 905ff.

9. Byrnside, N. C., Torvik, P. J. and Swift, H. F. (1972), "Impact Crater Formation at Intermediate Velocities", Journal of Basic Engineering, 1972, pp 398-399.

10. Johnson, W., Impact Strength of Materials, Edward Arnold, London; Crane, Russak, New York, 1972, Chapter 9.

11. Tate, A., "A Comment on a Paper by Awerbuch and Bodner Concerning the Mechanics of Plate Perforation by a Projectile", International Journal of Engineering Science, Vol. 17, 1979, pp 341-344.

12. Hill, R., "Cavitation and the Influence of Headshape in Attack of Thick Targets by Non-Deforming Projectiles", J. Mech. Phys. Solids, Vol. 28, 1980, pp 249-263.

13. Hopkins, H. G., "Dynamic Expansion of Spherical Cavities in Metals", I.N. Sneddon and R. Hill (Ed.), Progress in Solid Mechanics, Vol. I, North-Holland Publishing Company, Amsterdam; Interscience Publishers Inc. New York , 1960, chapter III.

14. Alekseevskii, V. P. , "Penetration of a Rod into a Target at High Velocity", Fizika Goreniya i Vzryva, Vol. 2, No. 2, 1966, pp 99-106, (Combustion, Explosion and Shock Waves, pp 63-66.)

15. Tate, A., "A Theory for the Deceleration of Long Rods After Impact", J. Mech. Phys. Solids, Vol. 15, 1967, pp 387-399.

16. Tate, A., "Further Results in the Theory of Long Rod Penetration", J. Mech. Phys. Solids, Vol. 17, 1969, pp 141-150.

17. Tate, A., "A Theoretical Estimate of Temperature Effects During Rod Penetration", The Proceedings of the 9th International Symposium on Ballistics, Part 2, 1986.

18. Christman, D. R. and Gehring, J. W., "Analysis of High-Velocity Projectile Penetration Mechanics", Journal of Applied Physics, Vol. 37, 1966, pp 1579-1587.

19. Rostoker, N., "The Formation of Craters by High-Speed Particles", Meteoritics, Vol. 1, No. 1, 1953, pp 11-27.

APPENDIX A

SHORT NON-ERODING (CONSTANT MASS) PENETRATORS

THIS PAGE INTENTIONALLY BLANK

Ideally, the relations listed below apply (in a strict sense) only to a rigid body penetrator, i.e. a penetrator that does not change its shape or its mass during the penetration phase. With minor misgivings, the equations are applicable to a deforming penetrator provided it is sufficiently short so that the major portion of the mass which has expanded radially retains a forward axial velocity. Taking Equation 9 of Section III:

$$H + k_0 \rho_t V^2 \tag{A-1}$$

as the target resistance, letting $k_0 = 1/2$ and adding a term which accounts for non-steady flow, we find the following expression for the pressure at the penetrator-target interface:

$$p_t = H + \frac{1}{2}\rho_t V^2 + \frac{1}{3}\rho_t D\frac{dV}{dt} \ . \tag{A-2}$$

This pressure is distributed over the presented area, $A = \pi D^2/4$, of the penetrator which is assumed to be constant or, at most, slowly varying. The mass, $M = A\ L\ \rho_p$, is taken to be constant. To a first approximation, the equation of motion for the penetrator-target system follows from balancing the axial forces:

$$M\frac{dV}{dt} = AL\rho_p V\frac{dV}{dx} = -A\ p_t \tag{A-3}$$

which can be integrated in a close form solution to produce Equation 11 of Section III. This equation is:

$$P(Z_0, Z) = L\frac{\rho_p}{\rho_t}\left(1 + \frac{\rho_t D}{3\rho_p L}\right) \ln\left(\frac{1+Z_0^2}{1+Z^2}\right) \tag{A-4}$$

where $Z^2 = p_t V^2/(2H)$ and $P(Z_0, Z)$ is the penetration depth when the instantaneous velocity is V. Z_0 is Z with V equal to the striking velocity V_0. The accompanying figures illustrate the penetrator-target intaraction described in this Appendix.

Equation A-4 is not applicable to situations where the shape factor k_0 is not constant during the penetration interaction. The value used here, 1/2, is applicable to a blunt nosed penetrator.

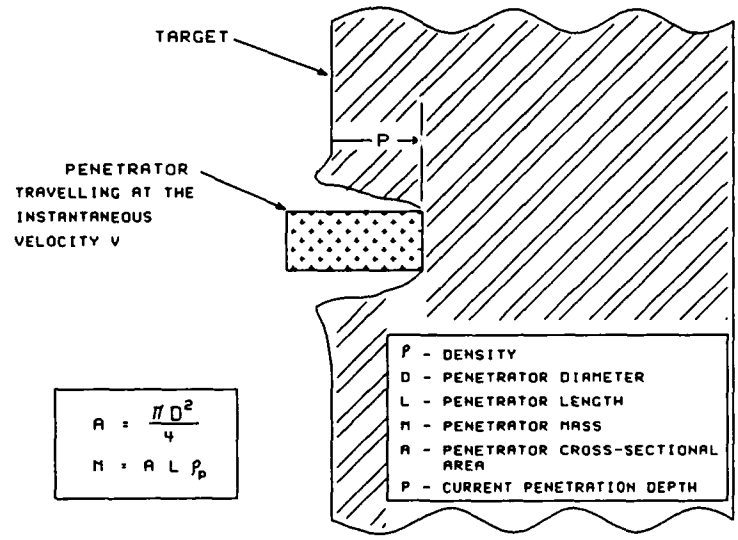

FIGURE A-1 Steady state interaction between a rigid right circular cylinder penetrator and a target.

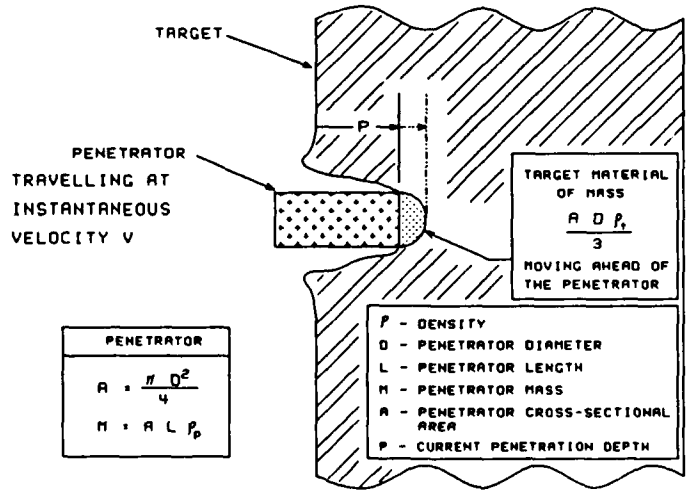

FIGURE A-2 Non steady state interaction between a rigid right circular cylinder penetrator and a target.

APPENDIX B

THE ALEKSEEVSKII-TATE MODEL FOR ERODING LONG ROD PENETRATORS

THIS PAGE INTENTIONALLY BLANK

B.1 Background

The one-dimensional eroding Long Rod Penetration Model as formulated independently by Alekseevskii and Tate is based on the following simplifying assumptions:

1. The dynamic behaviour of the homogeneous penetrator is that of a rigid body up to some pressure Y. Likewise, the homogeneous target acts as a rigid body up to some pressure H. The material flows like a fluid for pressures above Y for the penetrator or H for the target.

2. After an initial impact transient, the penetrator-target interface moves with a velocity U. If the penetrator erodes (becomes shorter than the initial length L_0 while penetrating the target) the tail end of the rigid portion of the penetrator has a velocity V while the front end has a velocity V - U relative to the interface.

3. The retardation of the rigid portion of the long rod penetrator (LRP) of length L is determined only by the pressure Y - the maximum stress level the still rigid rod material can sustain before it begins to act as a fluid.

The statements above are summarized by the following coupled differential equations (refer to Figure B-1 with respect to Equations B-1 and B-2):

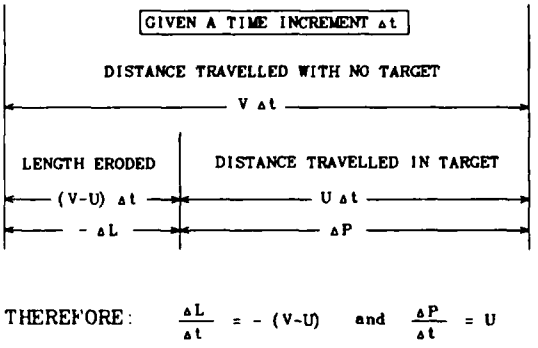

FIGURE B-1 Basis for dL/dt and dP/dt equations.

$$\frac{dP}{dt} = U \qquad \text{(B-1)}$$

$$\frac{dL}{dt} = -(V-U) \quad , \qquad \text{(B-2)}$$

$$A_p L \rho_p \frac{dV}{dt} = -Y A_p . \qquad \text{(B-3)}$$

In these equations, P is the depth of penetration, L is the instantaneous length, A_p is the penetrator cross-sectional area, and ρ_p is the penetrator density.

Up to this point, the Alekseevskii and the Tate formulations are identical. However, there are only three equations with four unknowns (P, L, U and V). So

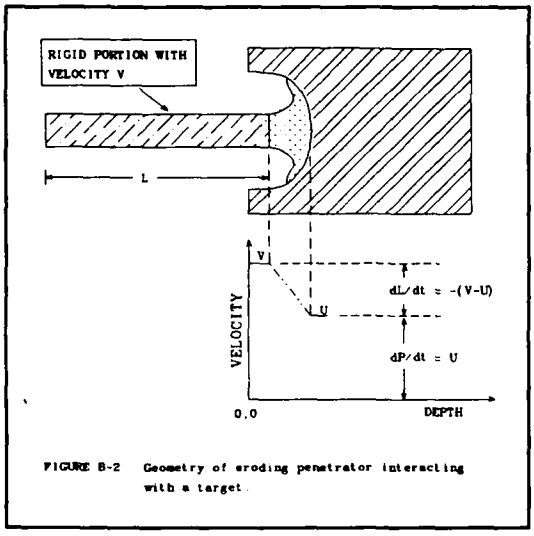

FIGURE B-2 Geometry of eroding penetrator interacting with a target.

an additional relation is needed to solve the system of equations.

Alekseevskii choses this relation to be the force (or pressure) balance across the penetrator-target interface:

$$A_p\left(Y+k_p\rho_p(V-U)^2\right)=A_p\left(H+k_t\rho_t U^2\right) \quad \text{(B-4)}$$

where k_p and k_t are shape factors which characterize the deformed regions in the penetrator and target materials near their respective rigid-fluid boundaries. In general, both of these factors are approximately 1/2.

Tate, on the other hand, uses a modified "Bernoulli Equation" for the stagnation pressure of two colliding fluid streams:

$$Y+\frac{1}{2}\rho_p(V-U)^2=\frac{1}{2}\rho_t U^2+R \quad . \qquad \text{(B-5)}$$

where Y and R have the same meaning as Alekseevskii's Y and H. When $k_p=k_t=1/2$, Equations B-4 and B-5 are identical. However, their physical justification is different.

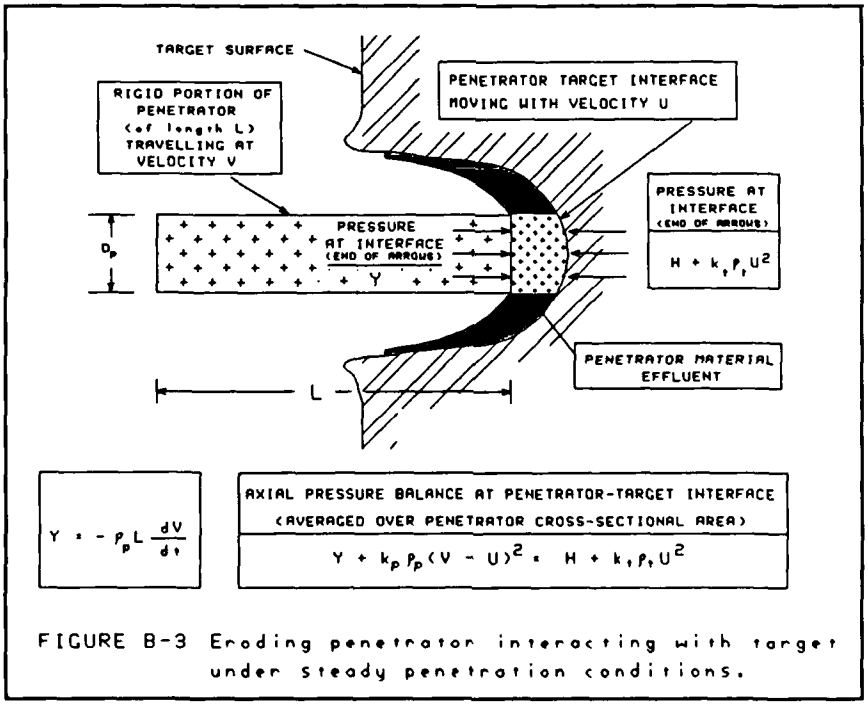

FIGURE B-3 Eroding penetrator interacting with target under steady penetration conditions.

Equation B-4 (or Equation B-5) delimits the special case of rigid target or of rigid penetrator behaviour:

a. Rigid target defined by U = 0, H ≥ Y and $V^2 \leq V_c^2 = \frac{H-Y}{k_p \rho_p}$. (B-6)

b. Rigid penetrator defined by (V - U) = 0, H ≤ Y and $V^2 = U^2 \leq \frac{Y-H}{k_t \rho_t}$. (B-7)

The regime of interest is that of the eroding penetrator and the target being penetrated, namely, (V - U) ≥ 0 and U ≥ 0. This corresponds to the velocity range $V_c \leq V \leq \infty$ or, equivalently, the parameter range $1 \geq \alpha \geq 0$.

Setting: $\alpha = \frac{H-Y}{k_p \rho_p V^2} = \frac{V_c^2}{V^2}$, and $\mu^2 = \frac{k_t \rho_t}{k_p \rho_p}$, (B-8,9)

the exact solution for U of the quadratic equation (Equation B-4) taking the negative sign of the radical is:

$$U = V \frac{1-\alpha}{1+\sqrt{\mu^2+\alpha(1-\mu^2)}} . \quad \text{(B-10)}$$

(Note that α is not constant, i.e., it is an inverse function of V.) To facilitate integrating Equations B-1 through B-3, it is necessary to use an approximate relation for U. Alekseevskii uses the approximate solution:

$$\frac{U}{V} \approx \frac{1}{1+\mu} - \frac{\alpha}{2\mu} \quad \text{(B-11)}$$

which diverges substantially from the exact solution near the cut-off velocity V_c unless $\mu \approx 1$. The cutoff velocity occurs when $\alpha = 1$ and where penetration ceases. At higher velocities, it is quite satisfactory. However, a better approximation is

$$\frac{U}{V} \approx \frac{1-\alpha}{1+\mu} \quad \rightarrow \quad \frac{V-U}{V} \approx \frac{\alpha+\mu}{1+\mu} \quad \text{(B-12)}$$

which yields the correct limit of U = 0 when $V = V_c$ (that is, $\alpha = 1$) and which differs by only a few percent from the more complicated exact solution (Equation B-10) over the velocity range of interest: $V > V_c$.

B.2 Erosion (change in length)

Combining Equations B-2 and B-3, the differential equation for the change in length can be expressed as:

$$dL = \frac{\rho_p L}{Y}(V-U)\,dV \quad . \tag{B-13}$$

Substituting the approximation (Equation B-12) for (V - U):

$$dL \approx \frac{\rho_p L}{2Y}\left[\frac{\mu+\alpha}{1+\mu}\right]2V dV \quad . \tag{B-14}$$

Setting: $$\eta = \frac{V^2}{V_0^2} \quad \text{whereby} \quad 2V dV = V_0^2\, d\eta \;; \tag{B-15}$$

$$\alpha_0 = \frac{H-Y}{k_p \rho_p V_0^2} = \frac{V_c^2}{V_0^2} \quad \rightarrow \quad \alpha = \frac{\alpha_0}{\eta} \;; \tag{B-16}$$

$$a_0 = \left(\frac{\rho_p V_0^2}{2Y}\right)\left(\frac{\mu}{1+\mu}\right) \;; \tag{B-17}$$

$$n = \frac{\rho_p V_c^2}{2Y(1+\mu)} = \frac{a_0 \alpha_0}{\mu} \tag{B-18}$$

and

$$2k_p n = \frac{H-Y}{Y(1+\mu)} \quad \rightarrow \quad Y = \frac{H}{1+2k_p n(1+\mu)} \;; \tag{B-19}$$

we obtain

$$\frac{dL}{L} = \left(a_0 + \frac{n}{\eta}\right)d\eta \quad . \tag{B-20}$$

Integrating this equation with the initial conditions ($L = L_0$, $V = V_0$, $\eta = 1$) and the condition ($L(1,\eta)$, V, η) at a later stage, the result is:

$$\frac{L(1,\eta)}{L_0} = \eta^{\,n}\, e^{-a_0(1-\eta)} \quad . \tag{B-21}$$

This equation is valid for all velocities between V_c and V_0, that is, $V_c \le V \le V_0$. At the cut-off velocity $V = V_c$ (when $U = 0$), the cut-off value for η is $\eta_c = n\mu/a_0$ and the length which remains (not eroded) is:

$$\frac{L(1,\eta_c)}{L_0} = \left(\frac{n\mu}{a_0}\right)^n e^{(n\mu - a_0)} \quad . \tag{B-22}$$

Equations B-21 and B-22 are valid for all values of n.

B.3 Penetration

Combining Equations B-1 and B-2 yields the differential equation for the change in penetration depth as a function of change of penetrator length:

$$dP = \frac{-U}{V-U}\,dL \approx \frac{-(1-\alpha)}{\mu+\alpha}\,dL \ . \qquad \text{(B-23)}$$

As a function of change of velocity (using Equation B-14), the change in penetration depth can be expressed as follows:

$$dP = -\frac{\rho_p L}{2Y}\left[\frac{1-\alpha}{1+\mu}\right]2V\,dV \ . \qquad \text{(B-24)}$$

Using Equations B-15 , B-17 and B-16, this becomes:

$$dP = -L\frac{a_0}{\mu}\left(1-\frac{\alpha_0}{\eta}\right)d\eta \ . \qquad \text{(B-25)}$$

Substituting $L(1,\eta)$ of Equation B-21 for L and using Equation B-18, Equation B-25 can be re-written as:

$$\frac{P(\eta)}{L_0} = -e^{-a_0}\int\left(\frac{a_0}{\mu}-\frac{n}{\eta}\right)\eta^{\,n}e^{a_0\eta}\,d\eta \ . \qquad \text{(B-26)}$$

By adding and subtracting $n\eta^{n-1}e^{a_0\eta}$ and multiplying both sides by μ, Equation B-26 can be partially integrated to yield:

$$\mu\frac{P(\eta)}{L_0} = Constant - \eta^{\,n}e^{a_0(\eta-1)} + n(1+\mu)\,e^{-a_0}\int\eta^{n-1}e^{a_0\eta}\,d\eta \ . \qquad \text{(B-27)}$$

The constant is evaluated by taking the initial conditions to be ($V=V_0$, $\eta=1$, $L=L_0$, $P=0$) and integrating to (V, η, L, $P(1,\eta)$; $\eta\geq\eta_c$). This results in:

$$\mu\frac{P(1,\eta)}{L_0} = 1-\eta^{\,n}\,e^{-a_0(1-\eta)} + n(1+\mu)\,e^{-a_0}\int_1^{\eta\geq\eta_c}\eta^{n-1}e^{a_0\eta}\,d\eta \qquad \text{(B-28)}$$

where $\eta_c = n\mu/a_0$ and $P(\eta\leq\eta_c) = 0$. Note that the second term to the right of the equal symbol is the same as Equation B-21.

Closed form solutions for integer values of n (n = 0,1,2,...) can be found. The expressions for $P(1,\eta)$ become progressively more complex as the value of n increases. The following segment evaluates the closed form solutions for n=0,1 and 2.

For n=0, Y = H and the velocities U and V are linearly related over the whole velocity range [that is, U = V / (1 + μ)] and are independent of the initial striking velocity V_0. Evaluating Equation B-28 with n = 0 results in:

$$\mu \frac{P(1,\eta)}{L_0} = 1 - e^{-a_0(1+\mu)} . \qquad \text{(B-29)}$$

This equation is equivalent to Equation 17 ($S_2(Z_0,Z)$) of Section III which is repeated here:

$$S_2(Z_0,Z) = \frac{1 - e^{\left(\frac{Z^2 - Z_0^2}{\mu(1+\mu)}\right)}}{\mu} \qquad \text{(B-30)}$$

where $Z_0^2 = \frac{\rho_t V_0^2}{2H}$ and $Z^2 = \frac{\rho_t V^2}{2H}$.

For n=1 and setting k_p = 1/2, i.e. $Y = \frac{H}{2+\mu}$, and integrating over the range of η = 1 to $\eta_c = \mu/a_0$, the result is:

$$\mu \frac{P(1,\eta_c)}{L_0} = 1 - \frac{\mu e^{(\mu - a_0)}}{a_0} + \frac{1+\mu}{a_0}\left(e^{(\mu - a_0)} - 1\right) . \qquad \text{(B-31)}$$

This is equivalent to Equation 19 of Section III which is:

$$S_3(Z_0,0) = \frac{1 - \frac{1+\mu}{a_0} + \frac{e^{(\mu - a_0)}}{a_0}}{\mu} \quad for\ \mu < a_0 \le \infty \qquad \text{(B-32)}$$

and $S_3(Z_0,0)$=0 for $a_0 \le \mu$.

For n=2 and setting k_p = 1/2, i.e. $Y = \frac{H}{3+2\mu}$, and integrating over the range of η = 1 to $\eta_c = 2\mu/a_0$,

$$\mu \frac{P(1,\eta)}{L_0} = 1 - \left(\frac{2\mu}{a_0}\right)^2 e^{(2\mu - a_0)} - \frac{2(1+\mu)}{a_0^2}\left(a_0 - 1 - (2\mu - 1)\, e^{(2\mu - a_0)}\right) . \qquad \text{(B-33)}$$

The **case n = ∞** corresponds to Y = 0, an LRP without any strength, which is represented by a "fluid rod". Equations B-1 through B-4 still apply but a different approach to the solution is required. Since Y = 0, there is no retardation of the portion of the rod which has not impinged on the target. So the velocity of the rod remains constant at V_0. The interface velocity U is still found from Equation B-12 but it also remains at a constant value U_0. However, its value is non-linearly dependent on V_0. Integrating Equations B-1 and B-2 with the

initial conditions at t = 0, P(t) = 0 and L(t) = L_0:

$$P(t) = U_0 t \ , \tag{B-34}$$

$$L(t) = L_0 - (V_0 - U_0)\, t \ . \tag{B-36}$$

This process continues until the length L is reduced to zero at a time $t_{max} = \frac{L_0}{V_0 - U_0}$. The maximum penetration occurs at t_{max} and is:

$$P_{max} = \frac{U_0}{V_0 - U_0} L_0 \ . \tag{B-36}$$

At any instant of time while penetration occurs, we have:

$$\frac{V_0 - U_0}{U_0} P(t) + L(t) = L_0 \ . \tag{B-37}$$

The exact solution (solved for in the manner of Equation B-10) and the approximate solution (refer to Equation B-12) are:

$$\frac{V_0 - U_0}{U_0} = \frac{\alpha_0 + \sqrt{\mu^2 + \alpha_0 (1 - \mu^2)}}{1 - \alpha_0} \approx \frac{\mu + \alpha_0}{1 - \alpha_0} \tag{B-38}$$

where $\alpha_0 = H/(k_p\, p_p\, V_0^2)$. Equation B-38, with $k_p = 1/2$, leads to the S_1 equation (Equation 16) of Section III which is:

$$S_1(Z_0) = \frac{Z_0 \sqrt{(Z_0^2 + 1 - \mu^2)} - \mu}{\mu (1 + Z_0^2)} \quad for\ Z_c < Z_0 \leq \infty \tag{B-39}$$

and $\quad S_1(Z_0) = 0 \quad for\ 0 < Z_0 < Z_c = \mu$.

Some additional insight into the penetration process can be obtained without integrating the system of differential equations. From Equation B-23:

$$dP = \frac{-U}{V - U} dL \ , \tag{B-40}$$

independent measurements of ΔP, ΔL, U and V can be used to deduce the values of H - Y from experimental observations assuming that the penetration process conforms approximately to Equations B-1 through B-4. Note that the H - Y value so determined, depends also on the shape factors k_p and k_t. The values for the shape factors can sometimes also be deduced from experimental observations.

Another useful relation can be deduced for the crater diameter (ignored in

this one dimensional treatment) by invoking the work-energy hypothesis. To an approximation, the energy lost by the rod is partitioned into work on the target (i.e., making a hole of diameter $D_t/D = h \geq 1$) and work to "fluidize" the rod. The energy balance at any instant of time is:

$$-\frac{d}{dt}\left(\frac{1}{2}\rho_p A_p L V^2\right) = A_t H U + A_p Y (V-U) \quad . \tag{B-41}$$

With $A_t/A_p = h^2 \geq 1$ and using Equations B-2, B-3, we obtain:

$$YV + \frac{1}{2}\rho_p (V-U) V^2 = h^2 H U + Y(V-U) \quad . \tag{B-42}$$

Using Equations B-8 and B-12, this can be expressed as:

$$h^2 = 1 + \frac{\rho_p V^2}{2H}\left(\frac{\mu+\alpha}{1-\alpha} - 2k_p\alpha\right) \quad . \tag{B-43}$$

For the special case of $k_p = 1/2$, this becomes:

$$h^2 = 1 + \frac{1}{2}\frac{\rho_p V^2}{H}\left(\frac{\mu+\alpha^2}{1-\alpha}\right) \quad . \tag{B-44}$$

which reduces to the well established experimental relation of h being approximately linearly dependent of V at very high velocities ($\alpha << 1$).

What has been assumed so far is that H and Y are constant. Some materials undergo large deformations in a rate dependent mode - they exhibit visco-plastic behavior. The H and Y values also depend on the shape of the penetrator/target interaction region that is only approximately described by the simple shape factors k_p and k_t. That Y can be treated as a constant is not obvious. As long as the crater cross-section made in the target is sufficiently large to allow for radial "flow" of material away from the eroding penetrator, the Y value is expected to be about equal to the stress of a penetrator cylinder loaded on an unconfined end, resulting in large deformations on that end (radial flow, "mush-room" formation). An estimate of the value of H can be determined from cavitation analysis (e.g., Hanagud, Ross[8] or Hopkins[13]).

Despite the limitations imposed by the assumptions, this simple LRP model is quite useful.

APPENDIX C

EXAMPLES OF PARAMETRIC VARIATION

This page intentionally blank.

The figures in this appendix are generated by using the following equations.

$$P(Z_0,0) = (L-mD)\,S_3(Z_0,0)+mD\,S_D(Z_0,0)\ , \tag{C-1}$$

$$S_3(Z_0,0)=\frac{1}{\mu}\left(1-\frac{1+\mu}{a_0}+\frac{e^{(\mu-a_0)}}{a_0}\right) \quad for\ \mu<a_0<\infty\ , \tag{C-2}$$

$$S_3(Z_0,0)=0 \quad for\ 0<a_0\le\mu\ ,$$

$$a_0=Z_0^2\left(\frac{2+\mu}{\mu(1+\mu)}\right) = \frac{\rho_p V_0^2}{2Y}\left(\frac{\mu}{1+\mu}\right)\ , \tag{C-3}$$

$$Y=\frac{H}{2+\mu}\ , \tag{C-4}$$

$$S_D(Z_0,Z)=\left(\frac{\rho_p}{\rho_t}+\frac{1}{3m}\right)\ln\left(\frac{1+Z_0^2}{1+Z^2}\right)\ , \tag{C-5}$$

$$Z=0 \quad ; \quad Z_0=V_0\sqrt{\frac{\rho_t}{2H}} \tag{C-6}$$

and

$$\mu=\sqrt{\frac{\rho_t}{\rho_p}}\ . \tag{C-7}$$

In these equations, $P(Z_0,0)$ is the depth of penetration into the target, L is the initial length of the penetrator, m is an empirical constant, D is the penetrator diameter, ρ_t is the target density, ρ_p is the penetrator density, H is target material resistance to penetration (units of pressure) and V_0 is the impact speed.

In the following figures, the target density, ρ_t, is 7850 kg/m^3, H = 5 GPa and m=2/3. The constants k_t, k_p and k_0 of Appendix A and Appendix B are each set to 1/2. The L/D ratio (denoted by f) takes on the vaules of 1, 2, 5, 10, 20, 50 and 100 for each respective curve. For each parameter plotted on the ordinate there are a pair of figures. The first of the pair is for ρ_p = 17300 kg/m^3 (corresponding to 91% tungsten alloy) with μ = 0.6736 and the second is for ρ_p = 18600 kg/m^3 (corresponding to DU-3/4Ti) with μ = 0.6496. The abscissa in all figures is impact velocity. The ordinate for each pair is as follows:

Figures C-1 and C-2: Penetration per unit length (P/L) evaluated from

$$\frac{P}{L} = \frac{m}{f} S_D(Z_0) + \left(1 - \frac{m}{f}\right) S_3(Z_0) ,$$

Figures C-3 and C-4: Penetration per unit diameter (P/D) evaluated from

$$\frac{P}{D} = m S_D(Z_0) + (f - m)\, S_3(Z_0) ,$$

Figures C-5 and C-6: Penetration per cube root of unit volume ($P/VOL^{1/3}$) evaluated from

$$\frac{P}{VOL^{\frac{1}{3}}} = \left(\frac{4}{\pi}\right)^{\frac{1}{3}} f^{\frac{2}{3}} \left[m S_D(Z_0) + \left(1 - \frac{m}{f}\right) S_3(Z_0)\right] ,$$

Figures C-7 and C-8: Penetration per cube root of unit kinetic energy ($P/E^{1/3}$) evaluated from

$$\frac{P}{E^{\frac{1}{3}}} = \left(\frac{8}{\pi \rho_p}\right)^{\frac{1}{3}} \left(\frac{f}{V}\right)^{\frac{2}{3}} \left[\frac{m}{f} S_D(Z_0) + \left(1 - \frac{m}{f}\right) S_3(Z_0)\right] ,$$

and

Figures C-9 and C-10: Penetration per cube root of unit mass ($P/M^{1/3}$) evaluated from

$$\frac{P}{M^{\frac{1}{3}}} = \left(\frac{4}{\pi \rho_p}\right)^{\frac{1}{3}} f^{\frac{2}{3}} \left[\frac{m}{f} S_D(Z_0) + \left(1 - \frac{m}{f}\right) S_3(Z_0)\right] .$$

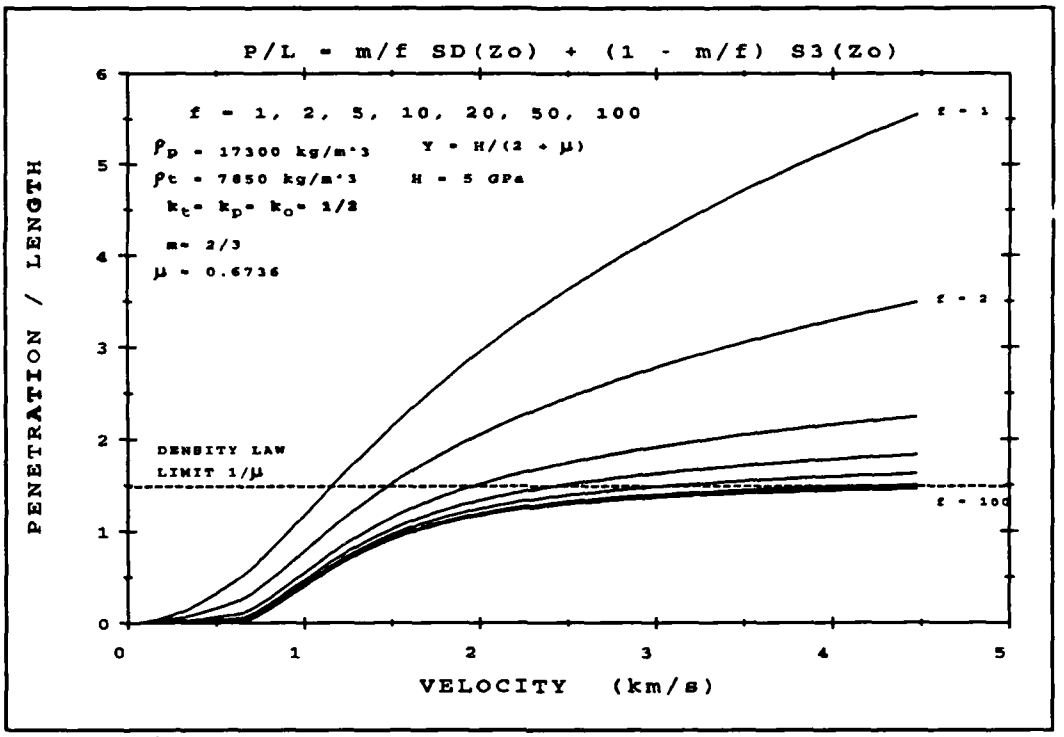

FIGURE C-1

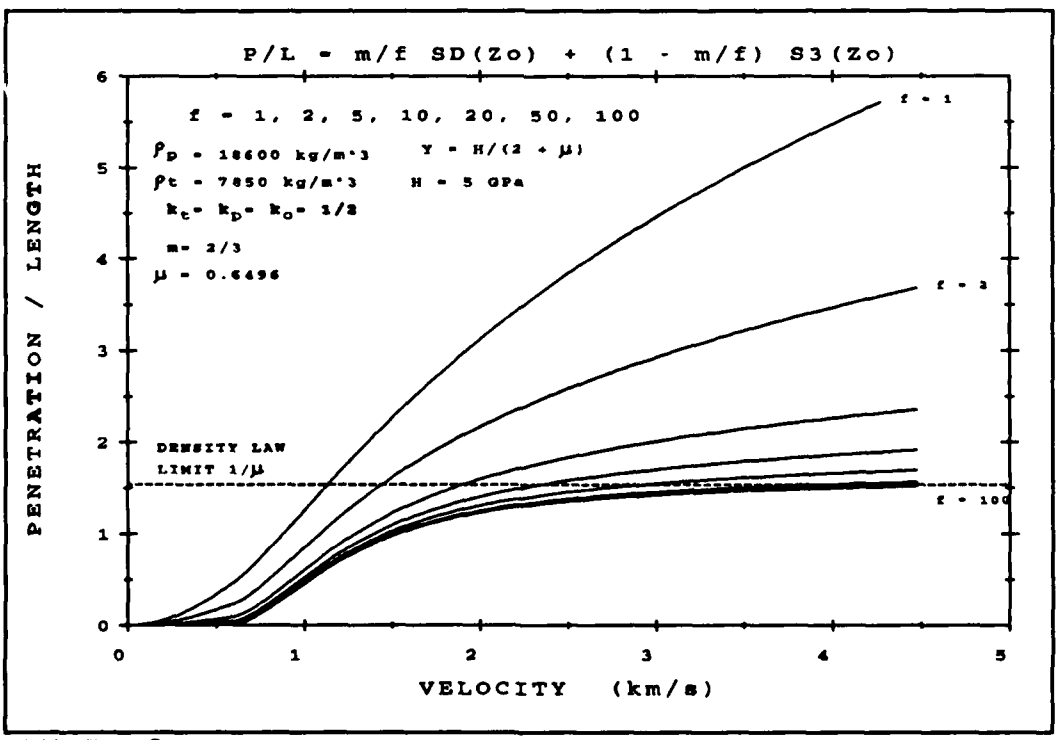

FIGURE C-2

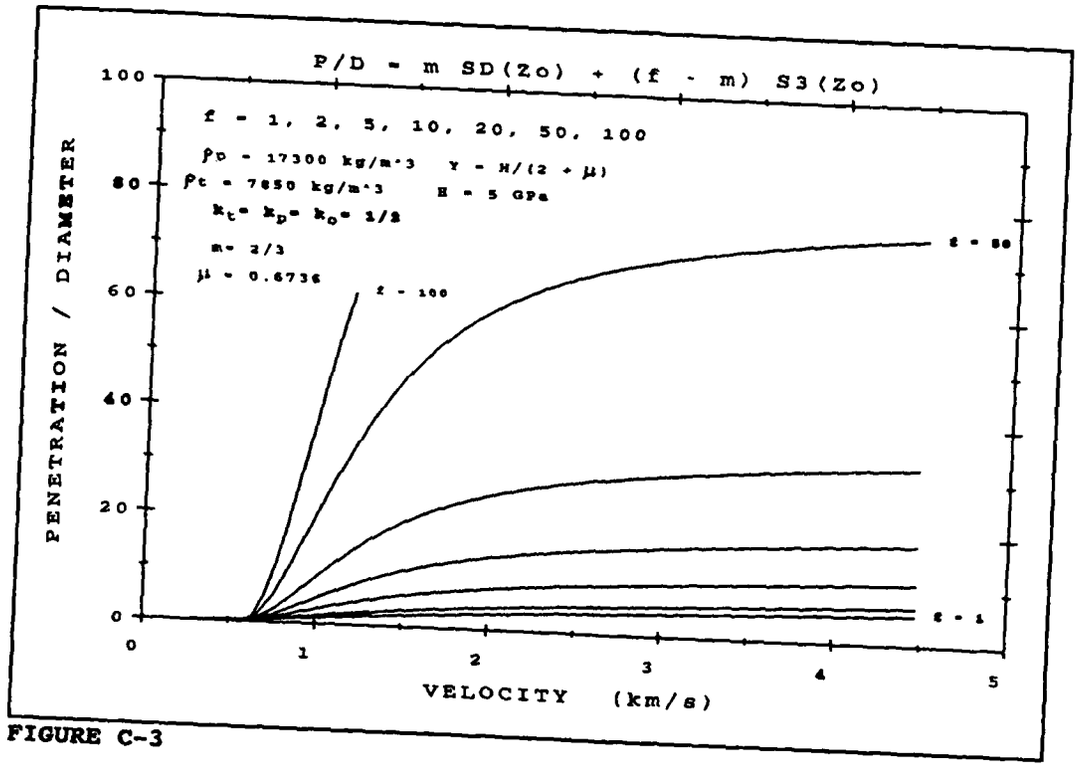

FIGURE C-3

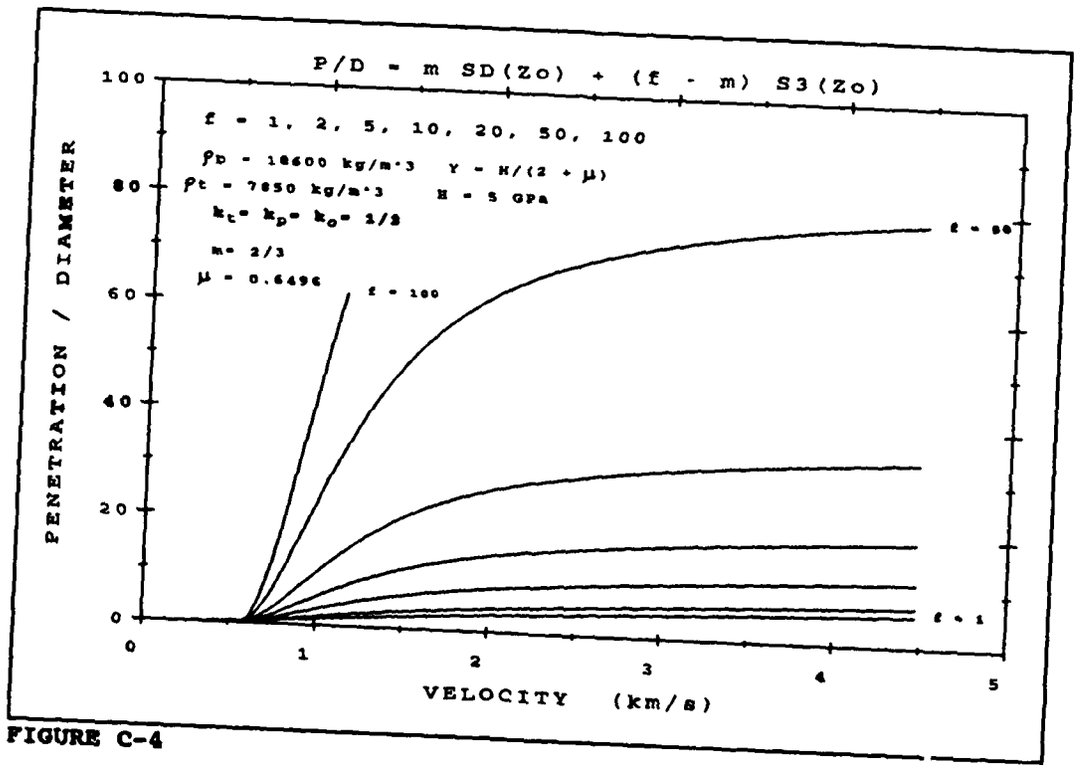

FIGURE C-4

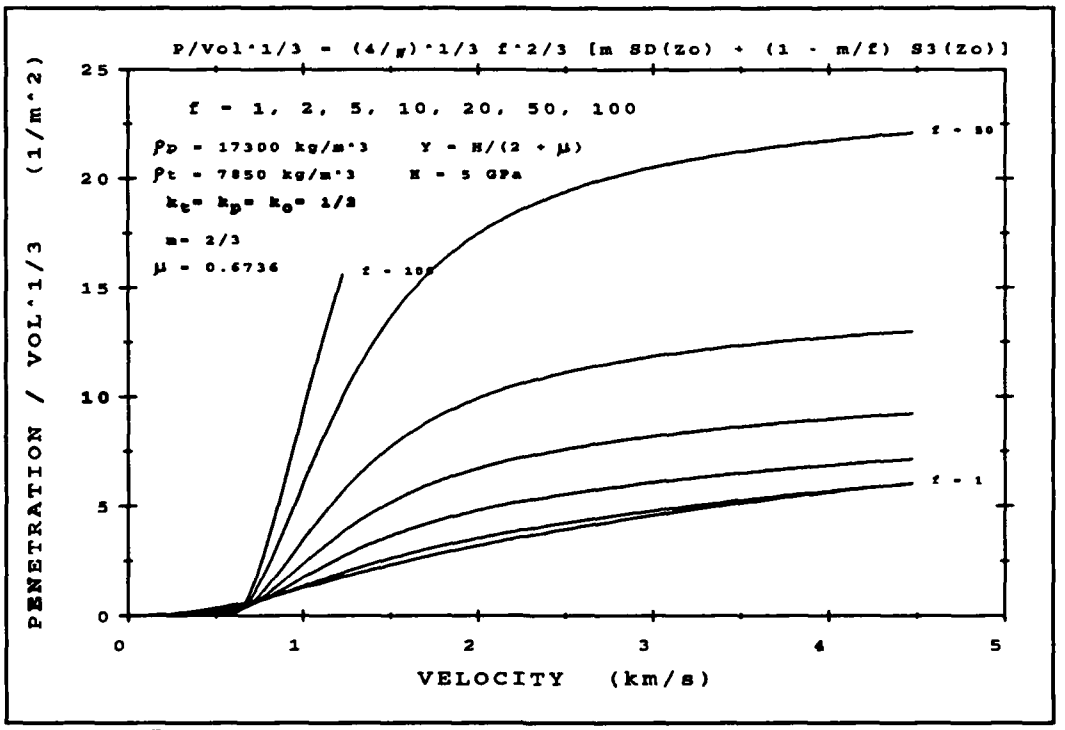

FIGURE C-5

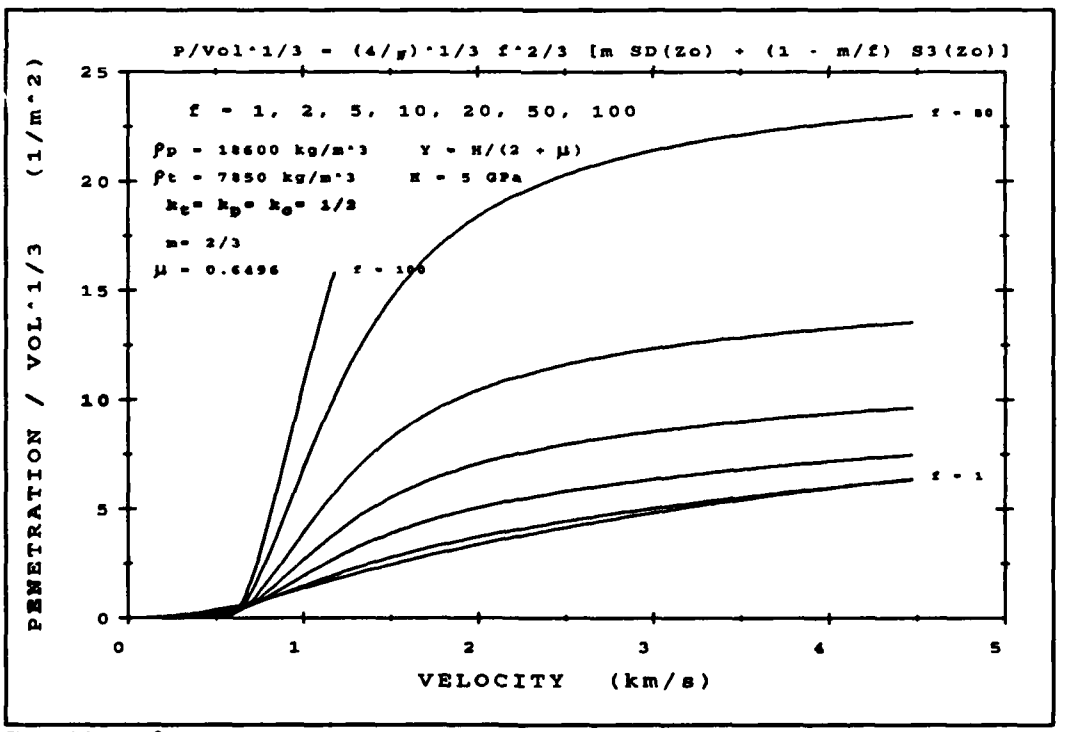

FIGURE C-6

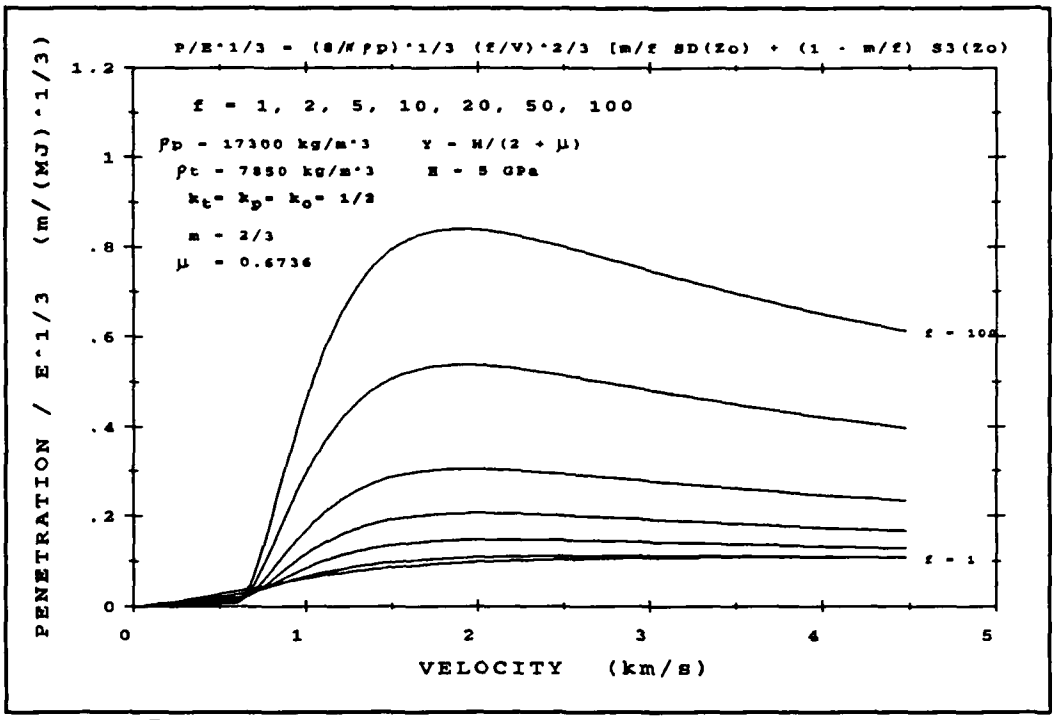

FIGURE C-7

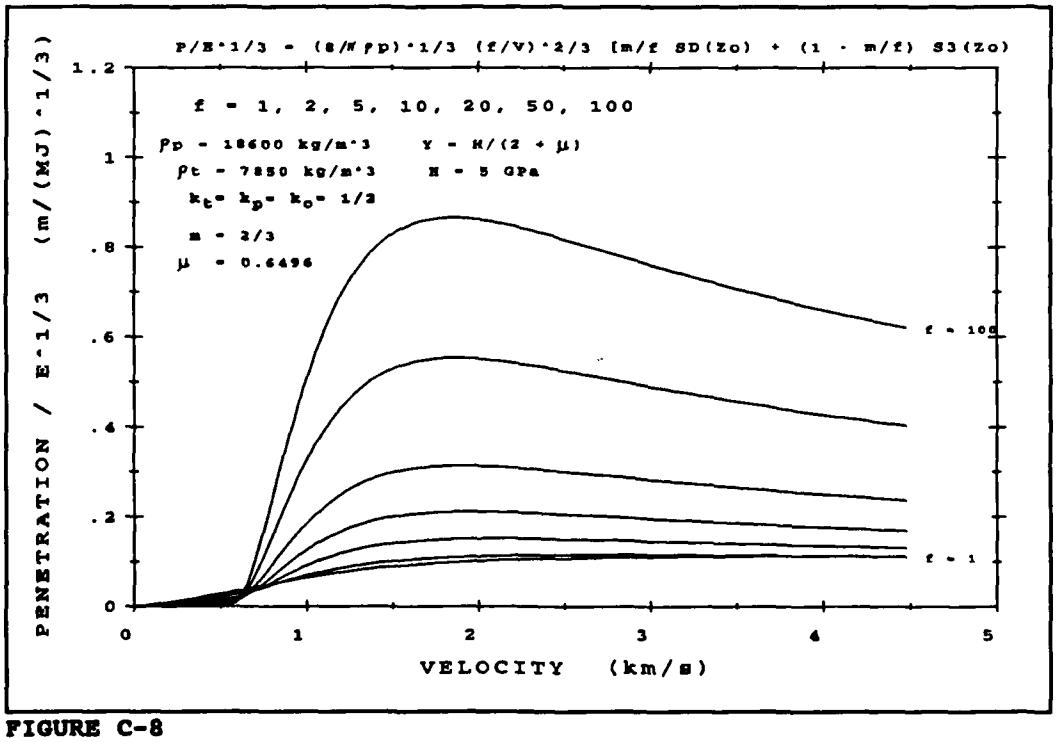

FIGURE C-8

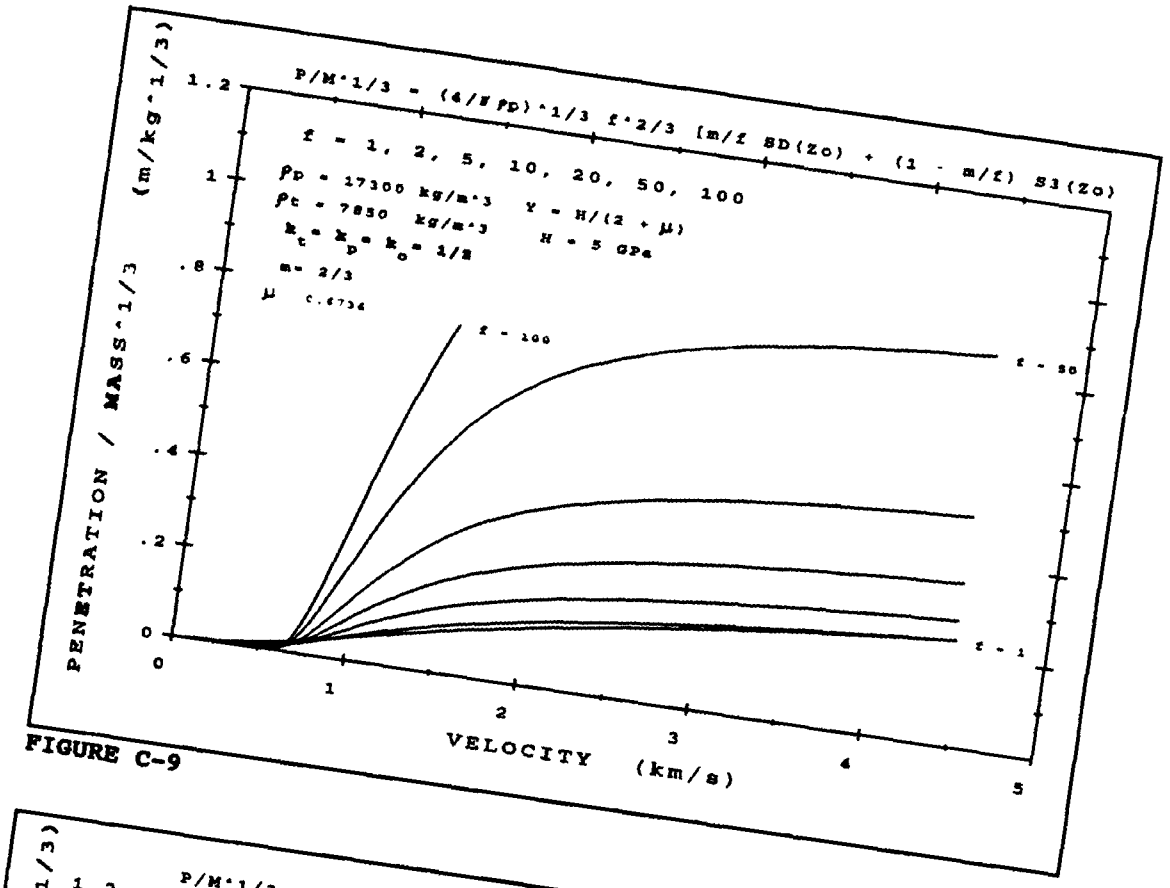

FIGURE C-9

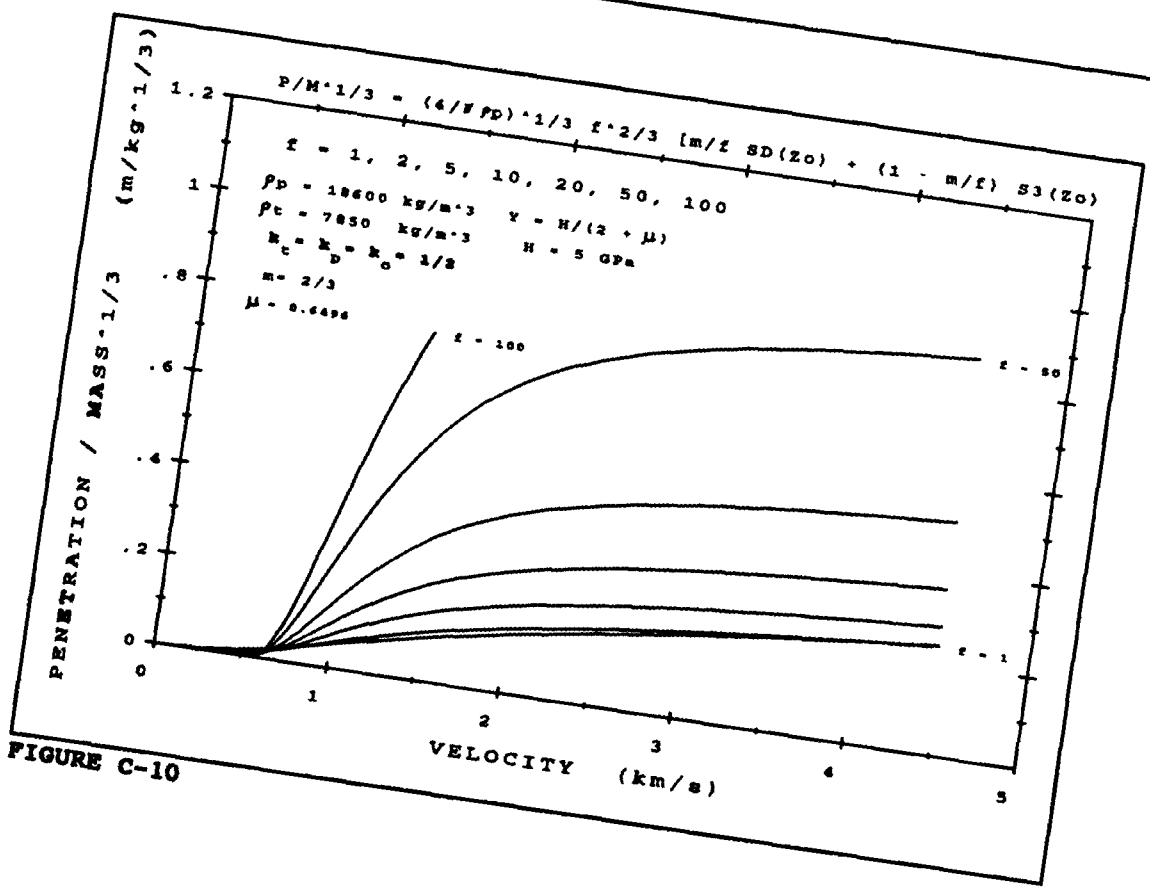

FIGURE C-10

No of Copies	Organization
2	Administrator Defense Technical Info Center ATTN: DTIC-DDA Cameron Station Alexandria, VA 22304-6145
1	HQDA (SARD-TR) WASH DC 20310-0001
1	Commander US Army Materiel Command ATTN: AMCDRA-ST 5001 Eisenhower Avenue Alexandria, VA 22333-0001
1	Commander US Army Laboratory Command ATTN: AMSLC-DL Adelphi, MD 20783-1145
2	Commander US Army, ARDEC ATTN: SMCAR-IMI-I Picatinny Arsenal, NJ 07806-5000
2	Commander US Army, ARDEC ATTN: SMCAR-TDC Picatinny Arsenal, NJ 07806-5000
1	Director Benet Weapons Laboratory US Army, ARDEC ATTN: SMCAR-CCB-TL Watervliet, NY 12189-4050
1	Commander US Army Armament, Munitions and Chemical Command ATTN: SMCAR-ESP-L Rock Island, IL 61299-5000
1	Director US Army Aviation Research and Technology Activity ATTN: SAVRT-R (Library) M/S 219-3 Ames Research Center Moffett Field, CA 94035-1000

No of Copies	Organization
1	Commander US Army Missile Command ATTN: AMSMI-RD-CS-R (DOC) Redstone Arsenal, AL 35898-5010
1	Commander US Army Tank-Automotive Command ATTN: AMSTA-TSL (Technical Library) Warren, MI 48397-5000
1	Director US Army TRADOC Analysis Command ATTN: ATRC-WSR White Sands Missile Range, NM 88002-5502
(Class. only) 1	Commandant US Army Infantry School ATTN: ATSH-CD (Security Mgr.) Fort Benning, GA 31905-5660
(Unclass. only) 1	Commandant US Army Infantry School ATTN: ATSH-CD-CSO-OR Fort Benning, GA 31905-5660
1	Air Force Armament Laboratory ATTN: AFATL/DLODL Eglin AFB, FL 32542-5000
	Aberdeen Proving Ground
2	Dir, USAMSAA ATTN: AMXSY-D AMXSY-MP, H. Cohen
1	Cdr, USATECOM ATTN: AMSTE-TD
3	Cdr, CRDEC, AMCCOM ATTN: SMCCR-RSP-A SMCCR-MU SMCCR-MSI
1	Dir, VLAMO ATTN: AMSLC-VL-D

INTENTIONALLY LEFT BLANK.

USER EVALUATION SHEET/CHANGE OF ADDRESS

This Laboratory undertakes a continuing effort to improve the quality of the reports it publishes. Your comments/answers to the items/questions below will aid us in our efforts.

1. BRL Report Number BRL-MR-3885 Date of Report FEBRUARY 1991

2. Date Report Received _____

3. Does this report satisfy a need? (Comment on purpose, related project, or other area of interest for which the report will be used.) _____

4. Specifically, how is the report being used? (Information source, design data, procedure, source of ideas, etc.) _____

5. Has the information in this report led to any quantitative savings as far as man-hours or dollars saved, operating costs avoided, or efficiencies achieved, etc? If so, please elaborate. _____

6. General Comments. What do you think should be changed to improve future reports? (Indicate changes to organization, technical content, format, etc.) _____

CURRENT ADDRESS

Name

Organization

Address

City, State, Zip Code

7. If indicating a Change of Address or Address Correction, please provide the New or Correct Address in Block 6 above and the Old or Incorrect address below.

OLD ADDRESS

Name

Organization

Address

City, State, Zip Code

(Remove this sheet, fold as indicated, staple or tape closed, and mail.)

---FOLD HERE---

DEPARTMENT OF THE ARMY
Director
U.S. Army Ballistic Research Laboratory
ATTN: SLCBR-DD-T
Aberdeen Proving Ground, MD 210[illegible] -5066
OFFICIAL BUSINESS

NO POSTAGE
NECESSARY
IF MAILED
IN THE
UNITED STATES

BUSINESS REPLY MAIL
FIRST CLASS PERMIT No 0001, APG, MD

POSTAGE WILL BE PAID BY ADDRESSEE

Director
U.S. Army Ballistic Research Laboratory
ATTN: SLCBR-DD-T
Aberdeen Proving Ground, MD 21005-9989

---FOLD HERE---